ELSEVIER

Contents lists available at ScienceDirect

Environmental Research

journal homepage: www.elsevier.com/locate/envres





Chemical characteristics of submicron particles in the Yellow Sea of Korea using aircraft measurements during the 2019–2023 period

Jinsoo Park ^a, Jinsoo Choi ^a, Junyoung Ahn ^a, Minyoung Sung ^a, Yonghan Jo ^a, Jiwon Seong ^a, Jiyun Jung ^a, Taehun Lee ^a, Jung Min Park ^a, Taehyun Park ^b, Jongho Kim ^c, Seokwon Kang ^b, Taehyoung Lee ^{b,*}

- ^a National Institute of Environmental Research, Climate and Air Quality Research Department, Incheon, South Korea
- ^b Hankuk University of Foreign Studies, Environmental Science, Yongin, South Korea
- ^c Hanseo University, Institute of Environment Research, Seosan-si, South Korea

ARTICLE INFO

Keywords:
Particulate matter (PM)
Sulfate (SO₄²)
Nitrate (NO₃)
Long range transport
Aircraft measurement

ABSTRACT

Air quality assessment is complex, as it reflects the interplay of local emissions and transboundary transport observed globally. In Korea, this complexity is manifested through contributions from mobile sources and the long-range transport of particulate matter from East Asia. Therefore, aircraft-based measurements have become essential for tracking and characterizing regional and transboundary pollution. Consequently, we examined longterm trends in aerosol concentration and chemical composition based on mass spectrometry data collected using a mid-sized research aircraft. Airborne measurements were conducted from 2019 to 2023 over the Yellow Sea during winter and spring using a Beechcraft 1900D equipped with high-resolution instruments for real-time analysis of particle- and gas-phase precursors. PM1 over the Yellow Sea was largely composed of oxidized organic aerosols, with oxidation levels increasing alongside PM1 concentrations. Sulfate concentrations declined over time, and ammonium sulfate was predominantly present as ammonium bisulfate ((NH₄)HSO₄)—indicating ammonium-deficient conditions. Further secondary formation is possible upon transport to inland regions with abundant NH₃. Air masses originating from eastern coastal China (Sector 3) and the Shandong region (Sector 4) exhibited elevated PM1 levels and higher fractions of nitrate and sulfate driven by enhanced secondary formation under elevated relative humidity and precursor concentrations. These findings suggest that the effect of the COVID-19 pandemic and emission reduction policies in China, particularly for SO2 and NH3, appear to be partly reflected in the composition and acidity of transported aerosols over the medium to long term.

1. Introduction

A wide range of anthropogenic activities, including energy production, vehicular emissions, fossil fuel combustion for residential heating, waste incineration, and biomass burning through incomplete combustion of organic matter, contribute to air pollution in East Asia (Wang et al., 2023a; Winijkul and Bond, 2016; Silva et al., 2013). To understand the complex impacts of these diverse anthropogenic emission sources, advanced analytical techniques have become essential for resolving the chemical composition and reaction processes of atmospheric aerosols. More recently, time-of-flight (ToF) mass spectrometry combined with aerodynamic and vacuum-based separation techniques has enabled real-time, high-resolution detection of particle and gas-phase pollutants (Zhang et al., 2024; Jensen et al., 2023; Park et al.,

2020; Hu et al., 2018; Laskin et al., 2012; McMurry, 2000). High-resolution aerosol mass spectrometry (HR-ToF-AMS) and related real-time techniques now allow detailed characterization of organic aerosol oxidation states and source influences (Hu et al., 2018; Zhang et al., 2024). Instruments such as the ToF-aerosol chemical speciation monitor (ToF-ACSM) and the soot-particle aerosol mass spectrometer (SP-AMS) provide high-resolution characterization of PM₁ composition. The ToF-ACSM conducts continuous measurement of non-refractory species such as sulfate, nitrate, ammonium, and organics, while the SP-AMS incorporates a laser vaporizer to additionally measure refractory black carbon (rBC) and associated coating material (Nault et al., 2025; Zografou et al., 2024; Farley et al., 2023). For the gas phase, proton-transfer-reaction ToF-MS (PTR-ToF-MS) enhances sensitivity to volatile organic compounds (VOCs) through an improved ion-molecule

E-mail address: thlee@hufs.ac.kr (T. Lee).

^{*} Corresponding author.

reactor, and ToF-chemical ionization mass spectrometer (ToF-CIMS). This allows selective, high-sensitivity detection of oxidized organic species and low-volatility compounds (Coggon et al., 2024; Li et al., 2024; Song et al., 2024).

While these advanced techniques have significantly improved the understanding of atmospheric aerosols, ground-based measurements are limited in the analysis of the vertical distribution and chemical reaction processes within the planetary boundary layer (PBL). To address this issue, advanced aircraft platforms and ship-based observations are being increasingly utilized. Particularly, aircraft measurements enable the collection of spatially extensive, high-frequency data across inaccessible regions, thereby offering critical insights into both local and transboundary pollution.

Recent studies have significantly advanced our understanding of aerosol sources and chemical transformation processes in East Asia. Ban et al. (2024) showed that biomass burning in an agricultural region of South Korea substantially increased particulate matter (PM) concentrations and organic chemical composition, thereby highlighting its role as a key local emission source modulated by meteorological conditions and burn practices. Fadnavis et al. (2024) used modelling, aircraft measurement, and satellite observations to show that South and East Asia have distinct emission sources and chemical signatures, which are associated with different climatic influences. Additional work also highlighted key features of aerosol chemistry, including seasonal variability, secondary formation, and the importance of long-distance transport for secondary aerosol aging in megacities of China (Zhong et al., 2022; Sun et al., 2015; Wang et al., 2015), and secondary organic aerosol production in South Korea (Nault et al., 2018). Despite these advances, most studies have been short-term intensive campaigns. This underscores the necessity of long-term airborne observations.

In Korea, air quality is influenced by local sources such as mobile emissions, fossil fuel combustion, and biomass burning, along with longrange transport of particulate matter from East Asia (Kang et al., 2025; Ban et al., 2024; Park et al., 2020; Nault et al., 2018). Therefore, aircraft-based measurements are essential for investigating regional and transboundary pollution. National Aeronautics and Space Administration (NASA) has conducted campaigns such as DISCOVER-AQ, to verify satellite air quality observations (Mazzuca et al., 2016; Anderson et al., 2014), and FIREX-AQ, to investigate biomass and agricultural fire emissions (Warneke et al., 2023; Johnson et al., 2021). These campaigns used platforms including the DC-8, Beechcraft King Air B200, and Lockheed Martin P-3B to observe gaseous precursors (NO, NO₂, CO, VOCs, O₃, etc.), PM, and particle number in real-time. In Europe, the DLR HALO aircraft was deployed in the EMeRGe campaign to monitor formaldehyde (HCHO), particle size distributions, and particle number over Europe and Asia (Förster et al., 2023; George et al., 2023). Korea's NIER has participated in international campaigns such as KORUS-AQ (2016), EMeRGe (2018), and ACCLIP (2021). The KORUS-AQ final report (NIER, 2020) estimated that transboundary PM2.5 contributed 40-80 % during high-concentration events, and highlighted the importance of secondary aerosol formation and polycyclic hydrocarbons. Since 2018, the YES-AQ campaign has also been conducted using the research vessel Gisang 1 to observe air pollutants over the Yellow Sea. To complement these efforts, in 2018, NIER developed a mid-sized aircraft platform that is equipped with instruments for both particleand gas-phase measurements. This enabled observations over the Yellow Sea, Seoul Metropolitan Area, Chungnam industrial complexes, and the East Sea. Additionally, this platform established Korea's independent capability for aircraft-based air quality monitoring, although its long-term applications have remained limited. To address this gap, the present study utilizes multi-year (2019-2023) airborne observations over the Yellow Sea to investigate PM1 concentration, chemical composition, oxidation state, and spatial distribution, with emphasis on the role of long-range transport from different source regions.

Despite the progress made through intensive international field campaigns, there remains a significant gap of multi-year airborne observations of fine particulate matter in East Asia. Previous campaigns such as KORUS-AQ, EMeRGe, and ACCLIP provided invaluable but short-term insights, which are insufficient to assess evolving source contributions or to establish long-term baselines. Our study addresses this gap by presenting the first multi-year (2019–2023) airborne dataset of PM_1 over the Yellow Sea. By integrating chemical composition, oxidation state, and spatial distribution analyses with a sector-based classification of air mass origin, this work provides new insights into the roles of long-range transport and atmospheric transformation. The significance of this study lies in establishing a long-term observational foundation to guide air quality management in Northeast Asia, while its contribution arises from the high-resolution airborne measurements to capture regional and transportation influences.

In this study, we utilized a mid-sized research aircraft to characterize the properties of fine particles transported into Korea from external regions. Airborne measurements were conducted over the Yellow Sea during winter and spring from 2019 to 2023. Trends in PM_1 (particulate matter with an aerodynamic diameter less than 1 μ m) concentration, chemical composition, and oxidation state were analyzed. For trends analysis, particular emphasis was placed on the chemical characteristics and spatial distribution of PM_1 , while focusing on the effects of longrange transportation by classifying source regions into sectors.

2. Materials and methods

2.1. Aircraft and instruments configuration

The aircraft used in this study was a modified 20-seat Beechcraft 1900D (Fig. 1), owned and operated by Hanseo University. The technical specifications of the aircraft are summarized in Table 1. Since its introduction to Korea in 2019, the Beechcraft 1900D has been based at the Taean Airfield of Hanseo University, which has served as the primary site for research flights. The airfield is equipped with essential facilities such as a dedicated runway for takeoff and landing, aviation fuel supply systems, maintenance support, and a hangar, thereby making it suitable for routine airborne observations (Ban et al., 2024).

To enable airborne air quality measurements, the aircraft was equipped with an isokinetic aerosol inlet (Droplet Measurement Technologies, USA) and a trace gas inlet (University of California, Irvine, USA) designed and installed in consideration of the aircraft's cruising speed. The aircraft was also outfitted with a digital air data probe (Aircraft Integrated Meteorological Measurement System; Aventech Research Inc., Ontario, Canada) to record meteorological parameters including latitude, longitude, altitude, temperature, relative humidity, and three-dimensional wind direction and speed during flight. Among the aircraft specifications, the maximum takeoff weight includes the combined mass of the aircraft, observation instruments, passengers, and fuel. Accordingly, the amount of fuel carried depends on the weight of onboard personnel and equipment. Under the operational conditions used in this study, the aircraft could fly for up to approximately 4 h per mission. In this work, forecast analysis was conducted prior to flights in order to avoid the cloudy weather and clouds cover and their consequent impact. Moreover, all flight measurements were carried out while staying away from clouds to prevent the influence of cloud water.

To enable high-resolution measurements of PM₁ concentration and chemical composition, the aircraft was equipped with instruments capable of collecting data at 1 Hz frequency. For aerosol-phase measurements, two primary instruments were deployed: a high-resolution time-of-flight aerosol mass spectrometer (HR-ToF-AMS; Aerodyne Research, USA) and a Single Particle Soot Photometer (SP2; Droplet Measurement Technologies, USA). For gas-phase observations, a proton transfer reaction time-of-flight mass spectrometer (PTR-ToF-MS; Ionicon Analytik, Austria) was used to measure VOCs, while a chemical ionization mass spectrometer (CIMS; University of California, Irvine, USA) was installed for sulfur dioxide (SO₂) detection. In addition, the aircraft was equipped with instruments to monitor other gas-phase



Fig. 1. Observation aircraft Beechcraft 1900D (B1900D).

Table 1Performance and specifications of B1900D.

Category	Performance and Specifications
Fuel	2519 L (360 kg/h)
Maximum takeoff weight	7765 kg
Maximum cargo capacity	1984 kg
Cabin height/width/length	1.8 m/1.38 m/7.67 m
Aircraft Height/width/wing length	4.7 m/17.6 m/17.6 m
Maximum flight altitude (Airborne measurement maximum flight altitude)	7620 m (≒ 3000 m)
Range (Range during the airborne measurement)	2306 km (≒ 900 km)
Power	AC 230 V (6 A, 50 Hz, 8
	Qty.)
Maximum aboard researcher	4 persons
Code/call sign	HL5238/Hanseo ECO

precursors, including nitrogen dioxide (NO_2) , ammonia (NH_3) , carbon monoxide (CO), carbon dioxide (CO_2) , methane (CH_4) , and ozone (O_3) . The layout of the instruments inside the aircraft is illustrated in Fig. 2, and detailed specifications of each instrument are provided in Table 2.

2.2. Aircraft flight measurement

Since the introduction of the aircraft in 2019, airborne measurements targeting particulate matter over the Yellow Sea have been conducted primarily during the winter (November-February) and spring (March-April) seasons, when high concentrations of long-range transported aerosols frequently occur. This study specifically focused on the flight segments conducted over the Yellow Sea. Fig. 3 presents the annual flight tracks over the Yellow Sea, while Table 3 summarizes the number of flights and total flight hours categorized by region, including the Yellow Sea, major emission sources, the Seoul Metropolitan Area, and the East Sea. Flights over the Yellow Sea were planned based on multiple meteorological and chemical forecast products-including weather data, radar images, environmental satellite, and chemical transport model outputs, such as GRIMS-chem (SNU AOD), ACMG AOD, GEOS-5 CO, and SIJAQ GIST (CMAQ vG)—that indicated potential transboundary pollution episodes. During these missions, the aircraft typically departed from the western boundary of the Korean Peninsula and flew westward to approximately 124°E longitude. Depending on the predicted transport direction of the incoming air masses, the aircraft then proceeded either northward or southward, followed by a vertical profiling segment at the northern or southern endpoint of the flight path.

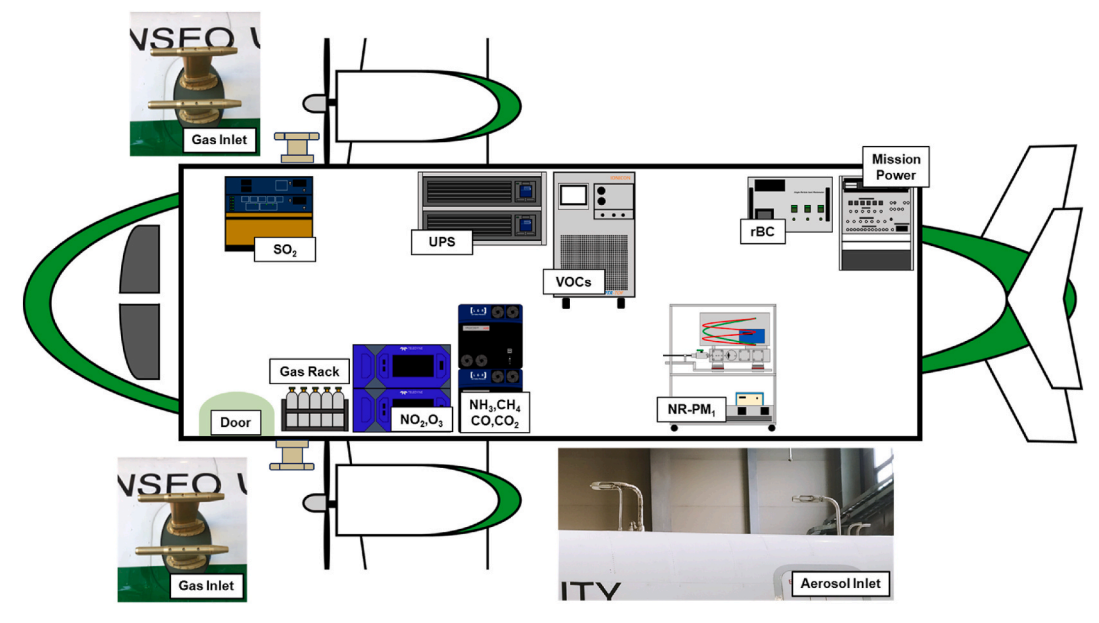


Fig. 2. Layout of instruments in aircraft; gas inlets were mounted in front of the aircraft propellers on both sides; aerosol inlet was installed on the top of the B1900D.

Table 2Configuration of instruments in aircraft.

Category	Instrument	Species
Gases	Proton Transfer Reaction Time of Flight Mass Spectrometer (PTR-ToF-MS)	Volatile Organic Compounds (VOCs); Benzene, Toluene, Xylene, Styrene, Acetaldehyde, Acetone, Acetic acid, Acetonitrile, Dimethyl sulfide, Isoprene, Methyl Vinyl Ketone, Methyl Ethyl Ketone, Pinene
	Off-Axis Integrated Cavity Output Spectroscopy (OA-ICOS)	Ammonia (NH ₃), carbon monoxide (CO), carbon dioxide (CO ₂), methane (CH ₄)
	Cavity Attenuated Phase Shift (CAPS)	Nitrogen dioxide (NO ₂)
	Chemiluminescence Chemical Ionization Mass Spectrometry (CIMS)	Ozone (O ₃) Nitric acid (HNO ₃), sulfur dioxide (SO ₂)
Particles	Single Particle Soot Photometer (SP2)	Refractory black carbon (rBC)
	High Resolution Time of Flight Aerosol Mass Spectrometer (HR- ToF-AMS)	Non-refractory particulate matter under the aerodynamic diameter of 1 µm (NR-PM ₁ ; Organics, nitrate, sulfate, ammonium, O:C, H:C etc.)
Meteorology and GPS	Aircraft Integrated Meteorological Measurement System (AIMMS-30, Air data probe)	Meteorology (Temperature, humidity, pressure, wind speed, wind direction), GPS (latitude, longitude, altitude)

2.3. High-resolution time of flight aerosol mass spectrometer (HR-ToF-AMS)

We employed a HR-ToF-AMS to investigate the chemical composition of particulate matter over the Yellow Sea via airborne observation. The operating principles of the HR-ToF-AMS have been described in detail in previous studies and the instrument has been widely used in both ground-based and aircraft-based measurements (Ban et al., 2024; Park et al., 2020). The HR-ToF-AMS provides real-time mass spectral analysis of non-refractory submicron aerosol particles (NR-PM₁; aerodynamic diameter $<1 \mu m$) and quantifies major chemical components including organics, sulfate, nitrate, ammonium, and chloride. It also enables the assessment of particle oxidation state and other key chemical characteristics (Bottenus et al., 2018; Nault et al., 2018; Li et al., 2015; Jimenez et al., 2009; DeCarlo et al., 2006). Aerosols are introduced into the instrument via an inlet and focused into a narrow beam through an aerodynamic lens. Thereafter, the particles pass through a drift region before being vaporized at ~600 °C in a thermal vaporizer. The vaporized molecules are subsequently ionized by electron impact at 70 eV. The resulting ions are separated by their mass-to-charge ratios in the ToF chamber based on differences in flight time. Each ion species was identified by its ToF signal, and concentrations were derived from the ion signal intensities (Zawadowicz et al., 2021). In this study, the HR-ToF-AMS was operated in fast mode to capture second-level resolution data while the aircraft traveled rapidly through different air masses. This configuration facilitated real-time analysis of the dynamic chemical composition of NR-PM1 during flight (Sullivan et al., 2019; Schroder et al., 2018).

2.4. Proton transfer reaction time of flight mass spectrometer (PTR-ToF-MS)

A PTR-ToF-MS was utilized to quantify VOCs in the atmosphere over the Yellow Sea in real time during airborne measurements. The operating principles of this instrument, as well as its applications across various platforms and study periods, have been widely documented in the literature (Coggon et al., 2024; Piel et al., 2019; Jordan et al., 2009).

The PTR-ToF-MS operates by generating hydronium ions (H_3O^+) in an ion source. As ambient air containing VOCs is introduced into the instrument, these compounds undergo proton transfer reactions with H_3O^+ ions in the drift tube. Subsequently, the protonated VOC molecules are separated based on their mass-to-charge ratios in the ToF chamber. The signal intensities of the separated ions are used to derive the concentrations of individual VOC species. During this study, ambient air samples collected from the upper atmosphere were drawn into the PTR-ToF-MS through a heated inlet line of approximately 1.5 m length. The sample flow rate was maintained at approximately 100 mL min $^{-1}$. VOC concentrations were measured with a temporal resolution of 1 s. Instrumental operating conditions in the drift tube were as follows: drift pressure = 2.4 mbar, drift temperature = 80 °C, mass range = m/z 18-200, and reduced electric field (E/N) = 132 Townsend $(1 \text{ Td} = 10^{-17} \text{ V cm}^2)$.

3. Results and discussion

3.1. Concentration variation of PM₁

Fig. 4 presents the annual variations in PM₁ concentration and chemical composition as measured during the study period. In 2019, the average PM₁ concentration was approximately 53 µg m⁻³, which decreased to 23 µg m⁻³ from 2020 onward—representing ~50 % reduction. Although concentrations slightly increased to 25 μg m⁻³ in 2021, they declined to 20 $\mu g \ m^{-3}$ again in 2022. In terms of chemical composition, the relative contributions of organics and ammonium remained relatively consistent between 18 and 20 % across years. However, sulfate (SO_4^{2-}) exhibited a decreasing trend from 23 to 8 %, whereas nitrate (NO₃) showed a gradual increase from 28 to 41 %. The chemical composition of PM₁ over the Yellow Sea showed increasing nitrate contributions in recent years. This trend is likely related to substantial reductions in SO2 emissions across East Asia, which have lowered sulfate formation and resulted in a relative increase in nitrate. In addition, the presence of sufficient NH3 and wintertime meteorological conditions favorable for the gas-to-particle partitioning of HNO3 may have further contributed to this enhancement. The continuous decline in SO₄²⁻ mass fraction was particularly evident over the years. This reduction is likely attributable to decreased energy consumption during the COVID-19 pandemic (bM. Li et al., 2021). In addition, past increases in coal consumption associated with China's rapid economic growth had contributed to elevated sulfate levels in atmospheric particulate matter. However, following the implementation of air quality improvement initiatives in China, including reductions in coal use, these efforts appear to have resulted in measurable decreases in sulfate concentrations (Wang et al., 2023b; Lu et al., 2010).

3.2. Relationships between aerosol chemical composition and gaseous pollutants based on pearson correlation analysis

Sector-based comparisons of NO₃, SO₄², and organic aerosol (OA) fractions were performed to characterize the chemical composition of PM₁ transported over the Yellow Sea (Fig. 5 and Table 4). Sector classification in this study was informed by regional wind directions, consistent with previous approaches for interpreting source impacts (Sun et al., 2015; Wang et al., 2015). This analysis was based on the top 50th percentile of observations during northern and southern flight paths over the Yellow Sea, with air mass classification determined by wind direction. Five sectors were defined with respect to the Korean Peninsula based on the direction of air mass transport and locations of presumed emission sources. Sector 1 corresponds to air masses originating from domestic inland regions of Korea primarily influenced by local anthropogenic emissions. Sector 2 includes air masses passing over the Yellow Sea and the East China Sea; this reflects the influence of marine boundary conditions and potential pollution from maritime transport. Sector 3 represents air masses transported from the eastern

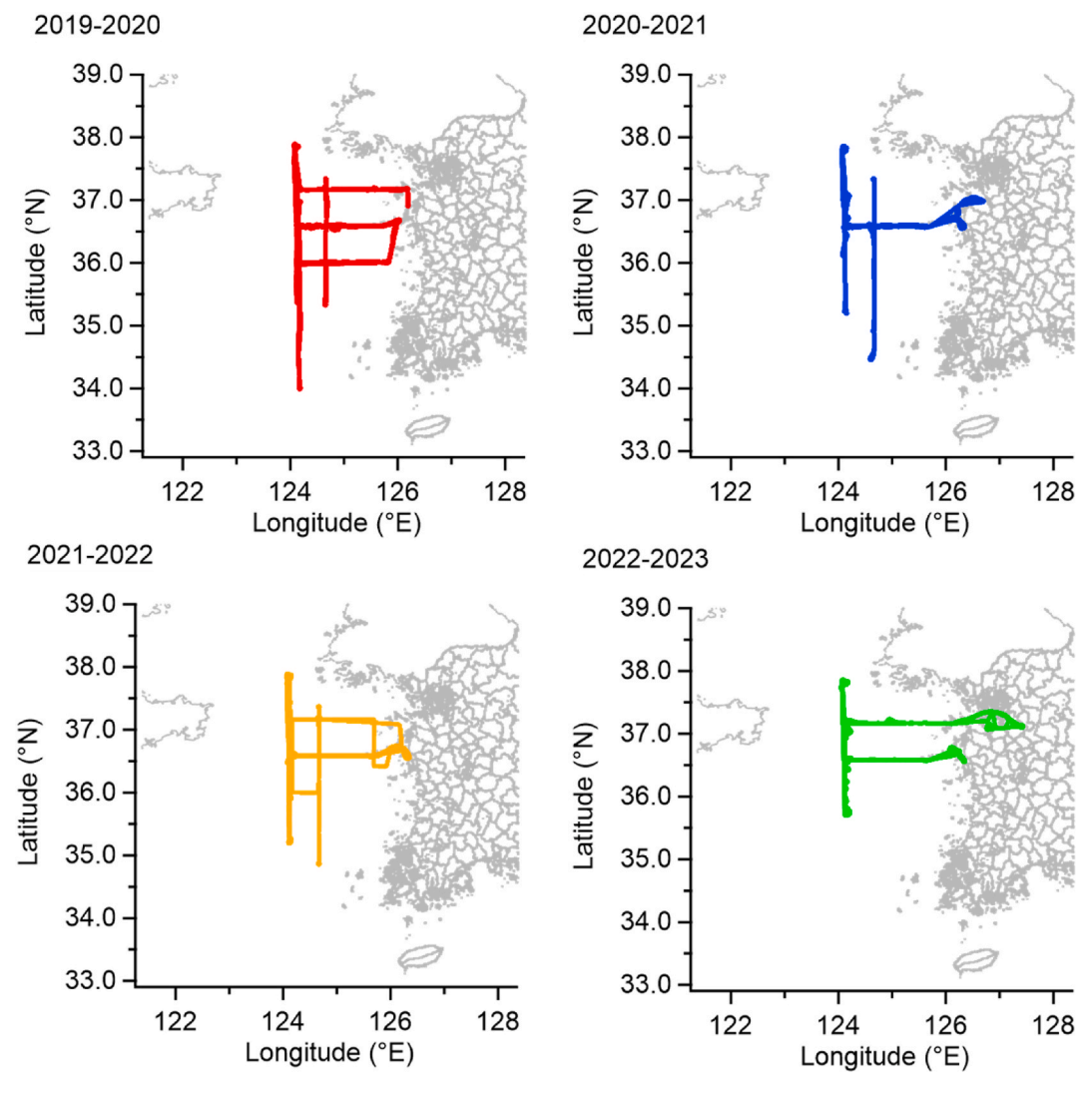


Fig. 3. Flight pathways each year.

Table 3Number of research flights each year in aircraft by targets.

Target	Number of research flights				
	19–20	20-21	21–22	22–23	
Yellow Sea	19	17	15	18	
Large Point Sources	6	5	2	4	
Seoul Metropolitan Area (SMA)	6	4	6	7	
East sea	-	4	7	4	
Total (times)	31	30	30	33	
Total (hours)	102	100	100	100	

coastal industrial areas of China, including highly urbanized and industrialized regions such as Shanghai and Qingdao. Sector 4 encompasses air masses from the Liaoning province region, which are known for intensive coal combustion and high emission densities (You et al., 2025). Sector 5 is associated with air masses arriving from the Bohai Bay area and northeastern industrial zones of China, including Manchuria, which are characterized by large-scale industrial activity and complex regional transport patterns.

Fig. 6 presents Pearson correlation coefficients (r) between airborne measurements of NR-PM₁ components, black carbon (BC), and various gaseous species including VOCs. Particle-phase species included total organics and the subgroups CxHy, CxHyO, and CxHyOz (representing

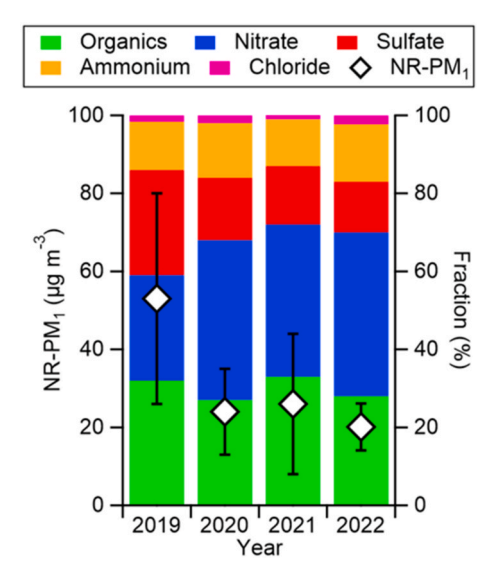


Fig. 4. Seasonal variations of concentration and chemical composition in $\ensuremath{\mathsf{NR}\text{-}\mathsf{PM}_1}.$

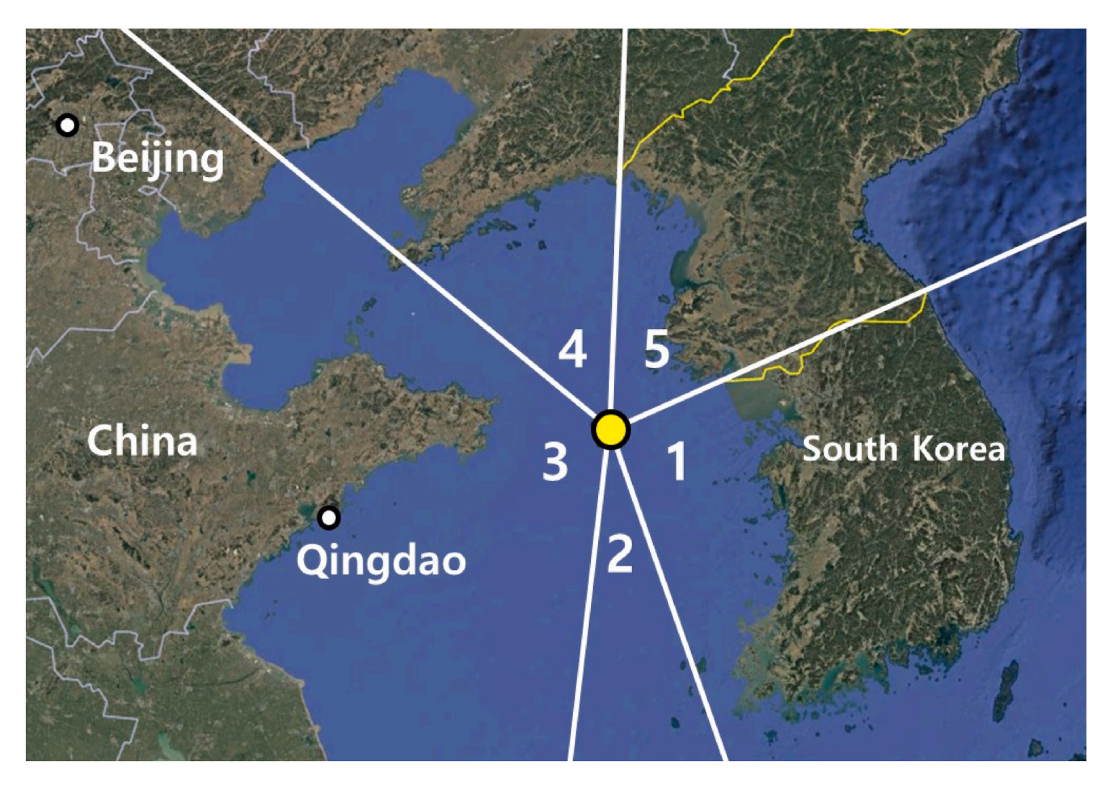


Fig. 5. Air mass trajectory sectoring by the wind direction of flight of Yellow Sea in Korea.

Table 4Number of research flights by classified sector based on the wind direction.

Sector	Location	Case	Year			
		#	19–20	20-21	21–22	22–23
1	South Korea	1	1	-	-	-
2	Yellow Sea	1	_	1	_	_
3	China (include Qingdao)	21	7	4	5	5
4	China (exclude Qingdao)	8	1	1	-	5
5	North Korea Total	5 36	2 11	- 6	2 7	1 11

different oxidation states); as well as NO_3^- , SO_4^{2-} , and NH_4^+ from HR-ToF-AMS; and rBC from SP2. The transformation from CxHy to more oxidized forms (CxHyO and CxHyOz) was used to assess the degree of organic aerosol aging. Gas-phase species included 11 VOCs (benzene, toluene, xylene, acetaldehyde, acetone, acetonitrile, isoprene, methyl vinyl ketone (MVK), methyl ethyl ketone (MEK), and pinene), along with NH₃, CO, CO₂, CH₄, SO₂, and HNO₃. Fig. 6 presents Pearson correlation coefficients (r) between airborne measurements of NR-PM₁ components, black carbon (BC), and various gaseous species including VOCs. To improve clarity, numerical r values are displayed within the figure, while the color coding (green for r > 0.5, red for r < -0.5, and gray otherwise) highlights relative strength of correlations.

The sector classification was applied to wind directions, and Sector 3 (covering Qingdao and eastern China) was chosen for detailed analysis (Fig. 5). This sector had the most frequent flight coverage from 2019 to 2023, and was therefore selected to represent long-range transport cases during this study period. Flights over the Yellow Sea were typically conducted on days with forecasted long-range pollution events. Annual variations in PM $_1$ composition within Sector 3 reflect changes in air mass characteristics arriving from eastern China. From 2019 to 2023, the fractions of nitrate (f_NO $_3$) and ammonium (f_NH $_4$) in NR-PM $_1$ increased annually, while the concentrations of SO $_4$ $_7$, f_SO $_4$ $_7$, SO $_2$, HNO $_3$, and NH $_3$ decreased. These trends are consistent with those of

emission inventory studies showing reduced agricultural NH3 use since 2012 due to changes in fertilizer type and total nitrogen application (Chen et al., 2022), and a steady decline in SO₂ emissions since 2005 following air quality control policies in China (Li et al., 2023). The observed increase in nitrate contribution suggests that long-range transport played an important role in shaping aerosol composition over the Yellow Sea. This is consistent with recent observations in coastal China, where SO₂ emissions and sulfate concentrations have markedly decreased following strict emission control measures, thereby leading to reduced sulfate and relatively enhanced nitrate contributions (Qi et al., 2023; Wen et al., 2023; Zheng et al., 2018). Therefore, this indicates that the compositional shift in PM₁ over Korea reflects not only local processes but also evolving source profiles in upwind regions. PM₁ and OA concentrations showed positive correlations with BC, CO2, and SO₂, while exhibiting negative correlations with f_CHOz—the most oxidized organic fragment (Ezani et al., 2021; Nakaishi, 2021). This suggests the presence of relatively fresh aerosols during flight observations. Previous studies have linked CxHy signals to hydrocarbon-like organic aerosol (HOA) from combustion emissions (Kang et al., 2025; He et al., 2018). Additionally, previous studies have reported that combustion-related organic aerosol can be influenced by both local emissions and long-range transport (Hayes et al., 2013). In this study, the elevated OA concentrations observed over the Yellow Sea likely reflect contributions from large-scale emission sources in eastern China.

 NO_3^- showed strong correlations with relatively stable tracers such as BC, CO, and CO_2 , and negative correlations with f_org. This supports the idea that long-range transported air masses underwent secondary formation processes en route leading to nitrate accumulation over the Yellow Sea (Zhong et al., 2022). SO_4^{2-} exhibited positive correlations with both relative humidity (RH) and SO_2 . Song et al. (2019) found that sulfate/ SO_2 ratios increase under high RH conditions, which suggested enhanced heterogeneous oxidation of SO_2 . SO_4^{2-} also correlated positively with benzene and negatively with the toluene/benzene (T/B) ratio. As benzene and toluene are both long-lived, high T/B ratios are typical near urban sources, while low ratios are indicative of aged, transported air masses (Raysoni et al., 2025; Sahu et al., 2020). These

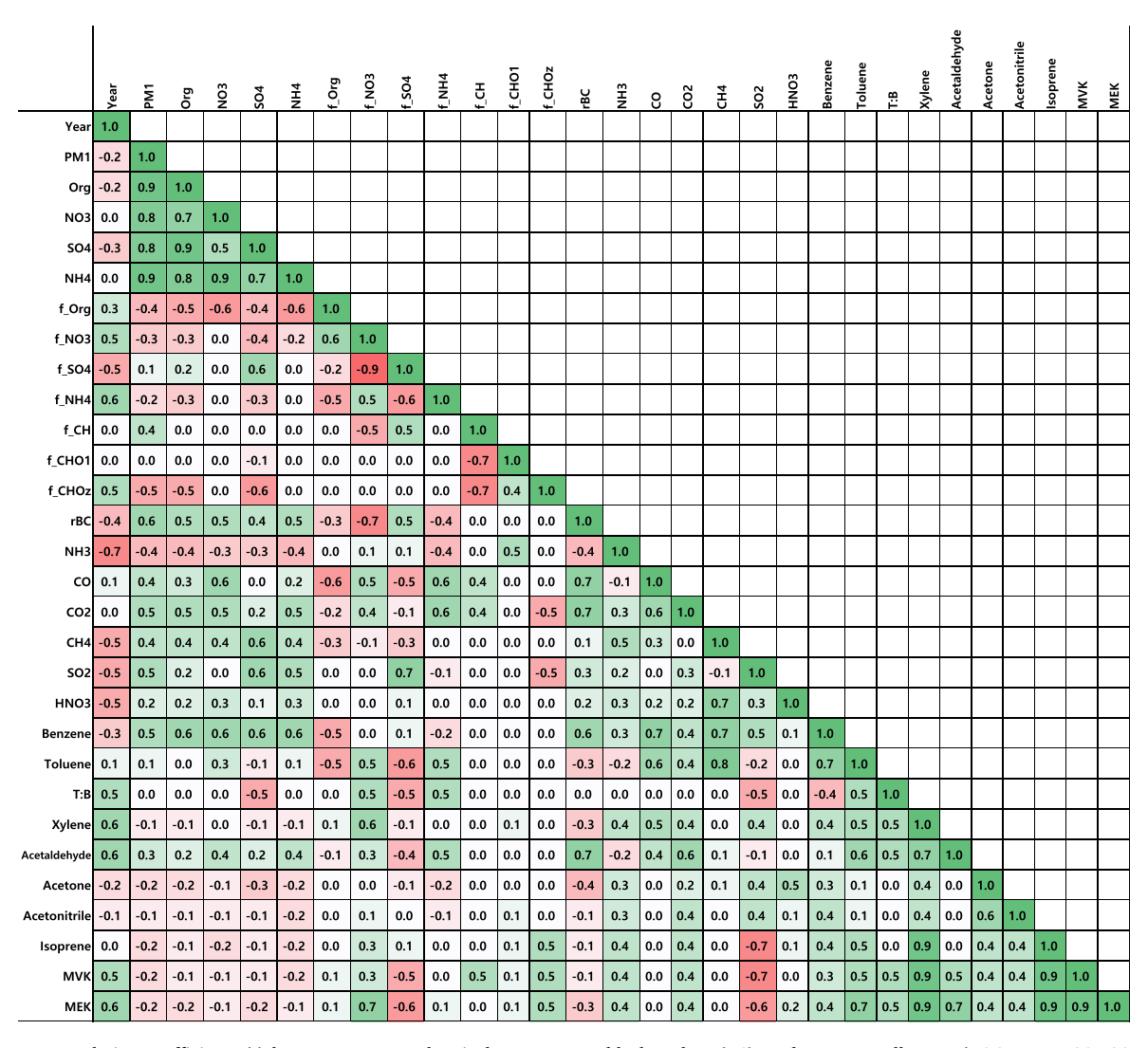


Fig. 6. Pearson correlation coefficients (r) between NR-PM₁ chemical components, black carbon (BC), and gaseous pollutants (VOCs, NH₃, CO, CO₂, CH₄, SO₂, HNO₃) measured during aircraft observations over the Yellow Sea. Circle colors indicate the direction of correlation (green: r > 0.5; red: r < -0.5; gray: $-0.5 \le r \le 0.5$). Numerical values inside the circles represent correlation coefficients. (For interpretation of the references to color in this figure legend, the reader is referred to the Web version of this article.)

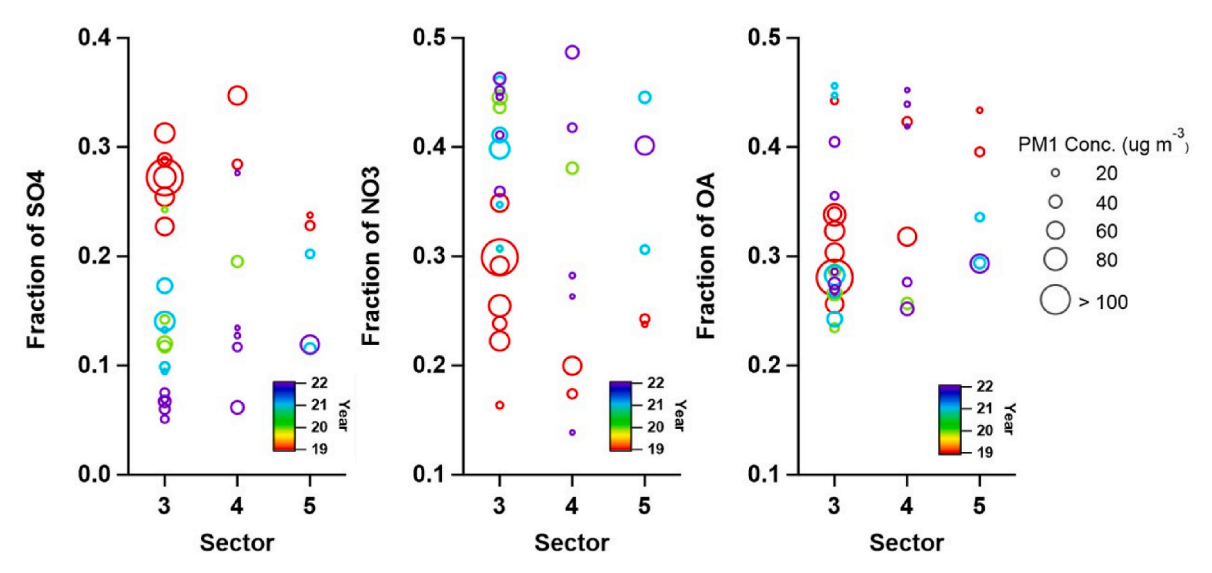


Fig. 7. Chemical compositions of the PM₁ by sector and year.

findings imply that elevated SO_2 from eastern China likely underwent heterogeneous reactions under humid Yellow Sea conditions, thereby promoting conversion to particle-phase sulfate during transport.

3.3. Analysis of chemical composition of PM_1 by sector

Fig. 7 presents a year-by-year comparison of SO_4^{2-} , NO_3^{-} , and OA mass fractions in PM_1 for selected long-range transport sectors, excluding those dominated by inland anthropogenic emissions and marine influences. The classification is based on air mass transport relative to the Baengnyeong Island. Circle color represents the observation year, while circle size reflects PM_1 mass concentration. Within each sector, SO_4^{2-} fractions exhibited a gradual increase from 2019 to 2022. Among the three sectors that were compared, a clear increasing gradient was observed from Sector 3 (influenced by the Beijing and the Shandong Peninsula). In contrast, NO_3^{-} fractions showed a decreasing trend over the same period. The relative fraction of NO_3^{-} was higher in Sector 3 than in Sector 4. Notably, PM_1 mass concentrations in Sector 3

were mostly higher than those in the other sectors, likely due to elevated emissions of NO_x from the eastern coastal regions of China (such as Shanghai, Tianjin, Guangzhou, etc.), which subsequently underwent photochemical conversion to NO_3^- during transport. In Sector 5 (influenced by the Bohai Bay and Manchuria), OA accounted for the higher average fraction among the three sectors, whereas SO_4^{2-} and NO_3^- fractions were comparatively low. PM_1 mass concentrations in this sector were also lower than those in the other sectors, thereby indicating that the air masses were likely influenced by background conditions and transported from relatively less polluted regions.

Overall, sulfate fractions were gradually decreased toward 2022, consistent with reported declines in SO_2 emissions in East Asia. In contrast, nitrate did not show a monotonic trend but exhibited relatively higher fractions in the period from 2020 to 2022, suggesting a shift in the inorganic aerosol balance as sulfate contributions decreased. OA fractions did not show a consistent long-term trend; instead, they varied by sector and year, with higher contributions occasionally observed in Sectors 4 and 5 during 2022, likely reflecting enhanced photochemical production. The largest PM_1 mass concentrations (>100 μg m⁻³)

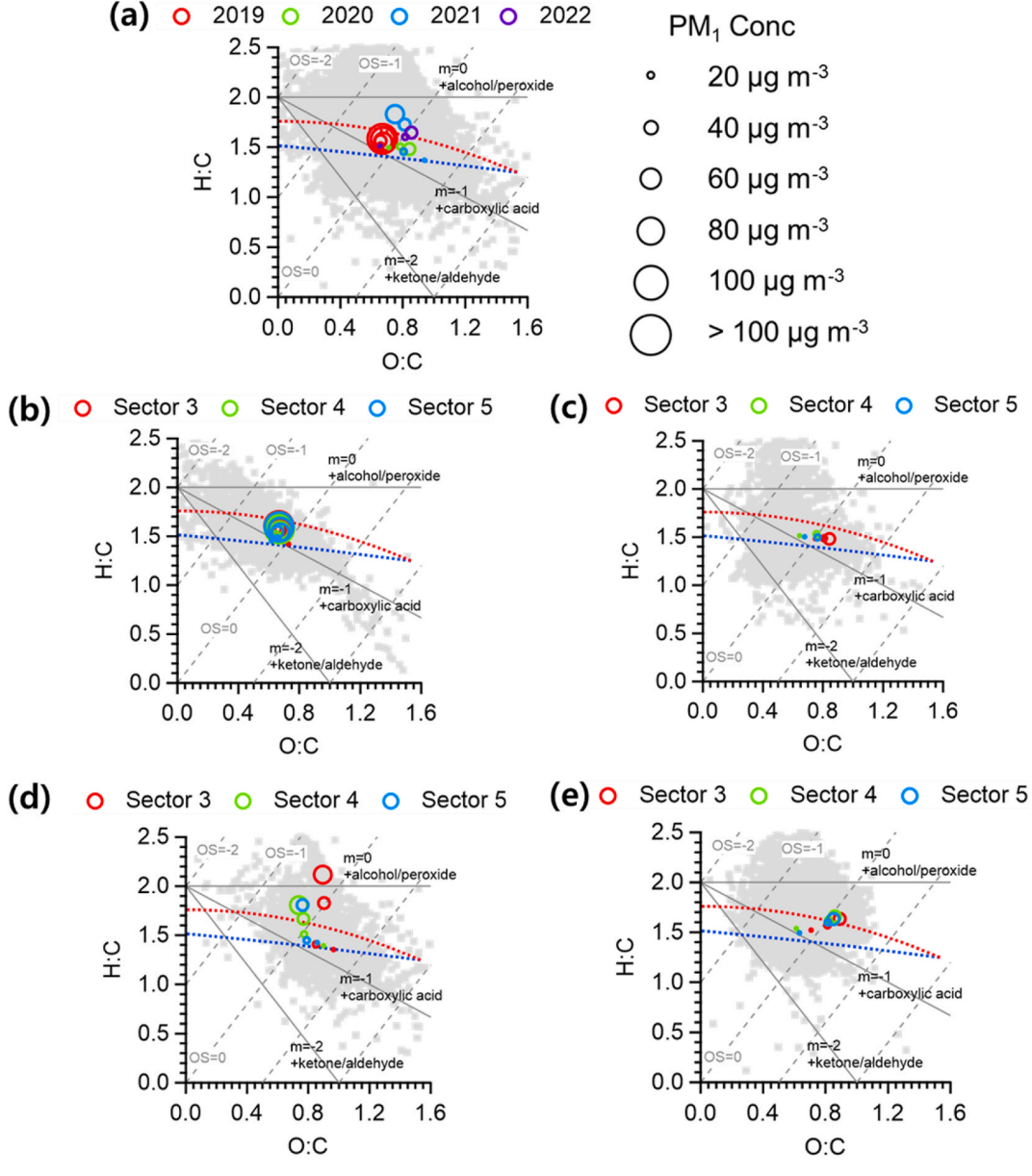


Fig. 8. Yearly variation in aerosol oxidation state: (a) total, (b) 2019, (c) 2020, (d) 2021, (e) 2022.

occurred primarily in Sector 3 during 2019, indicating the strong influence of long-range transported plumes during that year, whereas subsequent years were characterized by lower overall concentrations. These results highlight that sectoral differences in PM_1 composition are more strongly driven by interannual variability and source region characteristics rather than uniform long-term trends.

The Van Krevelen diagram illustrates the oxidative progression of organic compounds emitted from primary sources during atmospheric transport and aging. As oxidation proceeds, the hydrogen-to-carbon (H: C) ratio decreases while the oxygen-to-carbon (O:C) ratio increases. These trends can be interpreted using the oxidation state (OS) of carbon, which can be categorized based on a threshold of zero (Thapa et al., 2020; Heald et al., 2010). This method is particularly useful for distinguishing between primary organic aerosols (POA) and secondary organic aerosols (SOA). The slope m in the Van Krevelen space reflects how hydrogen atoms are substituted during oxidation: m = 0 indicates the addition of oxygen without hydrogen loss (e.g., formation of alcohols or peroxides), m = -1 corresponds to substitution with a carboxylic

acid group, and m=-2 implies substitution by ketone or aldehyde functional groups.

Fig. 8 presents changes in the oxidation state of organic aerosols observed over the Yellow Sea analyzed by year and sector. Fig. 8a shows annual averages of O:C and H:C ratios from 2019 to 2022. Across the study period, OA exhibited a mixture of fresh and oxidized characteristics, with oxidation states varying by year. In 2019 and 2021, OA tended to have higher H:C and lower O:C values, which is indicative of fresher organic matter. In contrast, 2020 and 2022 showed the opposite pattern—lower H:C and higher O:C ratios—suggesting greater oxidative processing. Throughout the entire period, high PM₁ concentrations were generally associated with high H:C and low O:C ratios, indicating the presence of relatively fresh OA. Conversely, lower PM₁ concentrations were linked with more oxidized OA. These results imply that highconcentration events may have been driven by the direct long-range transport of freshly emitted pollutants from China. Fig. 8(b-e) shows Van Krevelen plots by sector (Sectors 3, 4, and 5) for each year. In 2019, high PM₁ concentrations were observed across all three sectors, and the

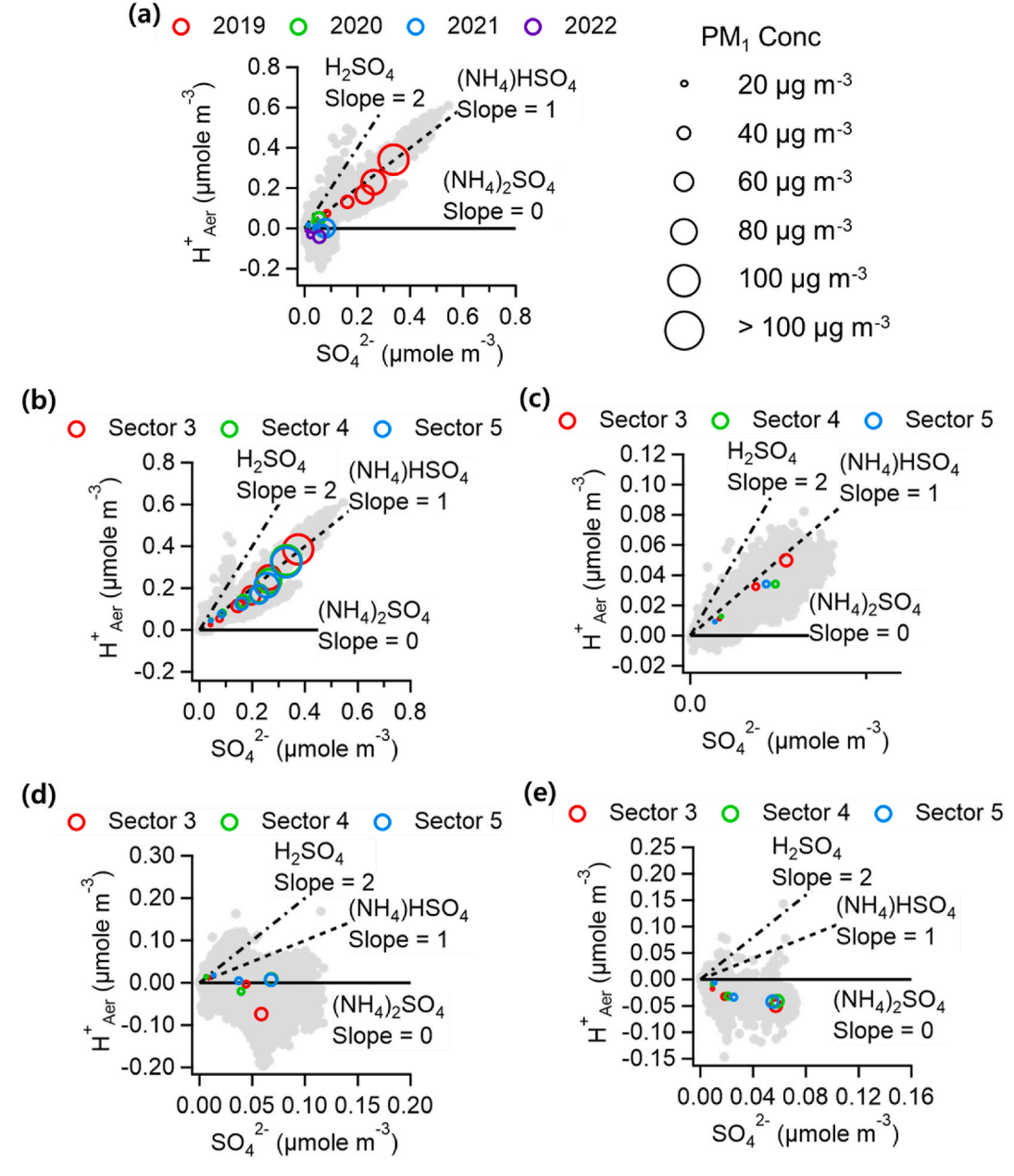


Fig. 9. Sulfate aerosol acidity classified by air mass trajectory for each year: (a) all years combined, (b) 2019, (c) 2020, (d) 2021, (e) 2022.

oxidation states of OA (O:C and H:C) were similar, thus indicating comparable chemical characteristics of air masses from these regions. In 2020, PM₁ concentrations decreased significantly relative to 2019, and O:C ratios increased overall. Sector 3 showed lower H:C and higher O:C values, thereby indicating more oxidized OA. In 2021, PM1 concentrations increased again, and all three sectors exhibited elevated oxidation levels. Notably, oxidation state (e.g., OSc and H:C) increased with PM1 concentration, especially in Sectors 3 and 4. In 2022, O:C values were generally high at elevated PM1 levels across all sectors, while H:C showed a slight increase, suggesting that oxidized OA dominated regardless of loading. These observations demonstrate that even within the same sector, OA oxidation states varied year to year influenced by differences in emissions, atmospheric conditions, and photochemical reactivity. The results highlight that the oxidative evolution of OA over the Yellow Sea is shaped by a combination of emission source characteristics, meteorological conditions, and the atmospheric oxidation environment. Long-range transport and changing oxidative capacity appear to play increasingly important roles in determining the chemical composition of PM₁ in this region.

Fig. 9 presents a comparison of the annual variation in the acid-base characteristics of sulfate-containing aerosols over the Yellow Sea analyzed according to the direction of incoming air masses. The concentration of aerosol-phase hydrogen ions (H_{Aer}^+) in NR-PM₁ was estimated through ion balance, considering the molar concentrations of NH₄⁺, NO₃⁻, SO₄²⁻, and Cl⁻, using the equation: $[H_{Aer}^+] = [NO_3^-] + 2[SO_4^2^-] + [Cl^-] - [NH_4^+]$ (Wu et al., 2020).

The slope between H_{Aer}^+ and SO_4^{2-} concentration serves as an indicator of aerosol acidity and the degree of neutralization. A slope of 2 corresponds to sulfuric acid (H_2SO_4), a slope of 1 indicates partially neutralized ammonium bisulfate ($(NH_4)HSO_4$), and a slope of 0 represents fully neutralized ammonium sulfate ($(NH_4)_2SO_4$). Consistent with the decreasing trend in sulfate concentrations and their fractional contribution to $NR-PM_1$ (as shown in previous sections), the results in Fig. 9 suggest that most sulfate aerosols over the Yellow Sea existed in the form of ammonium bisulfate. This form was particularly prevalent in 2019 and 2020, with average slope values across Sectors 3, 4, and 5 clustering near 1, which indicated a partially neutralized state.

These observations imply that acidic pollutants such as SO₂, largely emitted from China, were transported long distances and contributed to aerosol acidity over the Yellow Sea. In 2020, slight decreases in slope values in Sectors 4 and 5 suggest a modest increase in aerosol neutralization, potentially due to reductions in SO₂ and NO_x emissions in China. By 2021, slope values in Sectors 4 and 5 approached zero, indicating a transition to fully neutralized aerosol (ammonium sulfate). In contrast, Sector 3 exhibited a negative slope, while in 2022, negative slopes were observed in all sectors, thereby reflecting a further increase in aerosol neutralization. This interannual trend indicates a steady decline in sulfate-related aerosol acidity over time, likely driven by regional reductions in ammonia and acid gas emissions (Zhou et al., 2022). Changes in aerosol chemical composition and acid-base balance not only reflect evolving characteristics of long-range transported pollutants, but also have important implications for domestic air quality and the formation of secondary aerosols in Korea.

Pathak et al. (2009) analyzed the relationship between the molar ratio of ammonium to sulfate ([NH $^{\downarrow}_4$]/[SO $^{2}_4$]) and that of nitrate to sulfate ([NO $^{3}_3$]/[SO $^{2}_4$]) to determine the formation conditions of secondary inorganic aerosols via reactions involving NH $_3$. When the [NH $^{\downarrow}_4$]/[SO $^{2}_4$] molar ratio reaches 1.5, the formation of ammonium nitrate (NH $_4$ NO $_3$) via the gas-phase reaction between NH $_3$ and HNO $_3$ becomes clearly evident. Based on this threshold, a molar ratio below 1.5 is generally associated with heterogeneous reactions, while a ratio above 1.5 indicates homogeneous reactions. In heterogeneous reactions, distinct phases interact—typically, ammonium first reacts with H $_2$ SO $_4$ in the aqueous phase to form (NH $_4$) $_2$ SO $_4$ preferentially, followed by NH $_4$ NO $_3$ formation. In contrast, homogeneous reactions occur when sufficient NH $_3$ has already reacted with H $_2$ SO $_4$ to fully neutralize sulfate

(forming $(NH_4)_2SO_4$), and further NH_4NO_3 formation proceeds in the presence of excess NH_3 and NO_X .

Fig. 10 illustrates the variation in $[NO_3^-]/[SO_4^{2-}]$ as a function of $[NH_4^+]/[SO_4^{2-}]$ by year and PM₁ concentration. Throughout the study period, a majority of the observed conditions corresponded to [NH₄⁺]/ $[SO_4^{2-}]$ ratios above 1.5, indicating an ammonium-rich regime. This suggests that when air masses containing NH₃, NO_x, and SO₂ (likely emitted from China) are transported to inland regions of Korea, the formation of secondary inorganic aerosol (SIA) can continue, contributing to elevated PM concentrations. When examined by year, both the $[NH_4^+]/[SO_4^{2-}]$ and $[NO_3^-]/[SO_4^{2-}]$ ratios showed increasing trends. These findings align with previous reports on sulfate acidity: in 2019, when the highest PM₁ concentrations were observed, sulfate was present in a mildly acidic form. In subsequent years, as PM₁ concentrations declined, sulfate neutralization increased. This coincided with a transition toward more ammonium-rich conditions and an increased likelihood of homogeneous reactions, particularly in more recent years. Such trends are likely the result of changes in the composition and concentration of air pollutants emitted from major sources in China prompted by national emission control policies (Zhou et al., 2022; Liu et al., 2018). The progression from sulfate-dominant acidic aerosols to a more neutralized, ammonium-rich aerosol environment provides important insight into the evolving mechanisms of secondary aerosol formation and their implications for air quality in Korea. Figs. 9 and 10 represent complementary perspectives on aerosol acidity. Fig. 9, based on ion balance, demonstrates that aerosols remained acidic overall. However, Fig. 10 shows that the NH_4^+/SO_4^{2-} ratios increased in later years, indicating a greater degree of neutralization compared to earlier periods. Together, these results suggest that while aerosols were still acidic, their acidity was gradually moderated by enhanced ammonium neutralization.

4. Conclusions

This study quantitatively analyzed the changes in PM₁ concentration, chemical composition, and characteristics of long-range transported air pollutants over the Yellow Sea using aircraft-based measurements conducted from 2019 to 2023. Utilizing high-resolution instruments such as HR-ToF-AMS, PTR-ToF-MS, and SP2 installed on a mid-sized research aircraft, both particulate and gas-phase species were measured in real time to enable detailed assessment of chemical transformations in the upper atmosphere over the Yellow Sea. The analysis revealed that PM₁ concentrations and sulfate contributions gradually declined over the study period, whereas the fractions of NO₃ and OA remained constant or increased, thus indicating sustained or enhanced secondary formation. Sector-based classification showed that air masses originating from eastern coastal China and the Shandong Peninsula were associated with high PM₁ concentrations and elevated NO₃, SO₄²⁻, and OA fractions, along with lower oxidation states and higher f CH values; this reflects the influence of fresh emissions. In contrast, air masses from the Bohai Bay and Manchurian regions exhibited lower PM1 concentrations and more oxidized OA, thus, suggesting that photochemical aging during long-range transport played a dominant role.

Van Krevelen diagram analysis indicated interannual variability in OA oxidation, as represented by O:C and H:C ratios. These differences were attributed not only to meteorological conditions but also to evolving emission patterns in upwind regions. The increasing $[NH_4^+]/[SO_4^2-]$ and $[NO_3^-]/[SO_4^2-]$ molar ratios over time suggested a transition toward more neutralized sulfate and the predominance of homogeneous reaction conditions. This reflects some influence of emission reduction policies in China, particularly regarding SO_2 and NH_3 , on the formation pathways of secondary inorganic aerosols over Korea. Overall, this study provides a systematic characterization of air pollutant transport and atmospheric processing over Korean airspace. The findings offer important scientific insights for the quantitative assessment of transboundary pollution, improvement of air quality forecasting, and

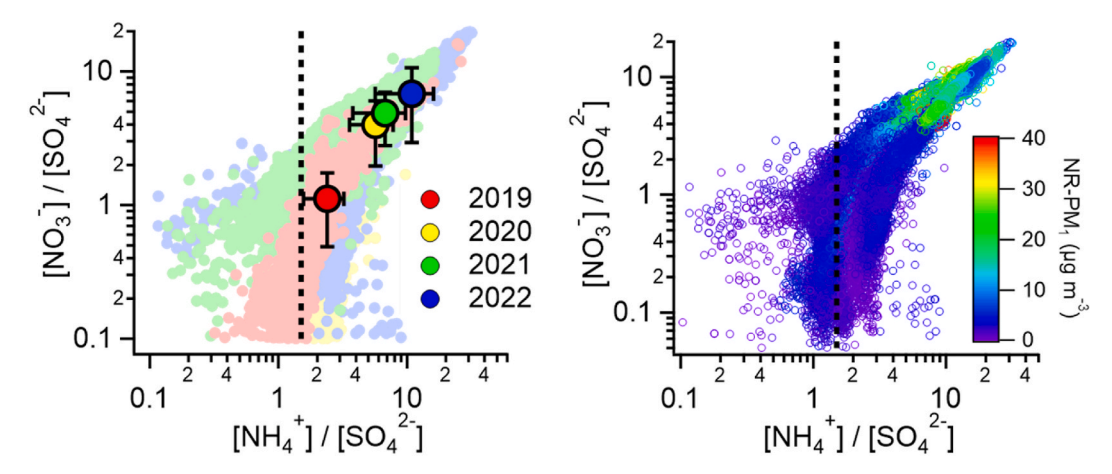


Fig. 10. Assessment of secondary inorganic aerosol formation regimes as a function of year and PM_1 concentration. The black dashed line represents the molar ratio of $[NH_4^+]$ and $[SO_4^{2-}]$ that divides heterogeneous and homogeneous reactions based on Pathak et al. (2009).

development of evidence-based policy strategies.

CRediT authorship contribution statement

Jinsoo Park: Writing – original draft, Project administration. Jinsoo Choi: Writing – review & editing, Project administration. Junyoung Ahn: Resources, Project administration. Minyoung Sung: Investigation. Yonghan Jo: Investigation. Jiwon Seong: Resources. Jiyun Jung: Investigation. Taehun Lee: Investigation. Jung Min Park: Resources. Taehyun Park: Writing – review & editing, Methodology, Investigation. Jongho Kim: Resources. Seokwon Kang: Writing – review & editing, Writing – original draft, Visualization, Methodology, Conceptualization. Taehyoung Lee: Writing – review & editing, Supervision, Conceptualization.

Declaration of competing interest

The authors declare that they have no known competing financial interests or personal relationships that could have appeared to influence the work reported in this paper.

Acknowledgments

This study was supported by the National Institute of Environmental Research (NIER) through a grant funded by the Ministry of Environment (MOE), South Korea (NIER-2025-01-01-013).

Data availability

Data will be made available on request.

References

Anderson, D.C., Loughner, C.P., Diskin, G., Weinheimer, A., Canty, T.P., Salawitch, R.J., Worden, H.M., Fried, A., Mikoviny, T., Wisthaler, A., Dickerson, R.R., 2014.
Measured and modeled CO and NOy in DISCOVER-AQ: an evaluation of emissions and chemistry over the eastern US. Atmos. Environ. 96, 78–87. https://doi.org/10.1016/j.atmosenv.2014.07.004.

Ban, J., Park, T., Kang, S., Choi, S., Wong, G., Choi, J., Seo, B.-K., Kim, S., Ahn, J., Lim, Y., Sung, M., Jung, S., Jung, J., Kim, H., Park, S.-M., Lee, J., Kim, J., Kim, J., Park, S.B., Park, J., Lee, T., 2024. Impact of biomass burning on air quality: a case study of the agricultural region in South Korea. Atmos. Environ. 339, 120864. https://doi.org/10.1016/j.atmosenv.2024.120864.

Bottenus, C.L.H., Massoli, P., Sueper, D., Canagaratna, M.R., VanderSchelden, G., Jobson, B.T., VanReken, T.M., 2018. Identification of amines in wintertime ambient particulate material using high resolution aerosol mass spectrometry. Atmos. Environ. 180, 173–183. https://doi.org/10.1016/j.atmosenv.2018.01.044.

Chen, Y., Zhang, L., Zhao, Y., Zhang, L., Zhang, J., Liu, M., Zhou, M., Luo, B., 2022. High-resolution ammonia emissions from nitrogen fertilizer application in China during 2005–2020. Atmosphere 13, 1297. https://doi.org/10.3390/atmos13081297.

Coggon, M.M., Stockwell, C.E., Claflin, M.S., Pfannerstill, E.Y., Xu, L., Gilman, J.B., Marcantonio, J., Cao, C., Bates, K., Gkatzelis, G.I., Lamplugh, A., Katz, E.F., Arata, C., Apel, E.C., Hornbrook, R.S., Piel, F., Majluf, F., Blake, D.R., Wisthaler, A., Canagaratna, M., Lerner, B.M., Goldstein, A.H., Mak, J.E., Warneke, C., 2024. Identifying and correcting interferences to PTR-ToF-MS measurements of isoprene and other urban volatile organic compounds. Atmos. Meas. Tech. 17, 801–825. https://doi.org/10.5194/amt-17-801-2024.

DeCarlo, P.F., Kimmel, J.R., Trimborn, A., Northway, M.J., Jayne, J.T., Aiken, A.C., Gonin, M., Fuhrer, K., Horvath, T., Docherty, K.S., Worsnop, D.R., Jimenez, J.L., 2006. Field-deployable, high-Resolution, time-of-flight aerosol mass spectrometer. Anal. Chem. 78, 8281–8289. https://doi.org/10.1021/ac061249n.

Ezani, E., Dhandapani, S., Heal, M.R., Praveena, S.M., Khan, M.F., Ramly, Z.T.A., 2021. Characteristics and source apportionment of Black Carbon (BC) in a suburban area of Klang Valley, Malaysia. Atmosphere 12, 784. https://doi.org/10.3390/ atmos12060784.

Fadnavis, S., Sonbawne, S.M., Laakso, A., Ploeger, F., Rap, A., Heinold, B., Sabin, T.P., Müller, R., 2024. Long range transport of South and East Asian anthropogenic aerosols counteracting Arctic warming. npj Climate and Atmospheric Science 7, 101. https://doi.org/10.1038/s41612-024-00633-1.

Farley, R.N., Collier, S., Cappa, C.D., Williams, L.R., Onasch, T.B., Russell, L.M., Kim, H., Zhang, Q., 2023. Source apportionment of soot particles and aqueous-phase processing of black carbon coatings in an urban environment. Atmos. Chem. Phys. 23, 15039–15056. https://doi.org/10.5194/acp-23-15039-2023.

Förster, E., Bönisch, H., Neumaier, M., Obersteiner, F., Zahn, A., Hilboll, A., Kalisz Hedegaard, A.B., Daskalakis, N., Poulidis, A.P., Vrekoussis, M., Lichtenstern, M., Braesicke, P., 2023. Chemical and dynamical identification of emission outflows during the HALO campaign EMeRGe in Europe and Asia. Atmos. Chem. Phys. 23, 1893–1918. https://doi.org/10.5194/acp-23-1893-2023.

George, M., Andrés Hernández, M.D., Nenakhov, V., Liu, Y., Burrows, J.P., Bohn, B., Förster, E., Obersteiner, F., Zahn, A., Harlaß, T., Ziereis, H., Schlager, H., Schreiner, B., Kluge, F., Bigge, K., Pfeilsticker, K., 2023. Airborne observations of peroxy radicals during the EMeRGe campaign in Europe. Atmos. Chem. Phys. 23, 7799–7822. https://doi.org/10.5194/acp-23-7799-2023.

Hayes, P.L., Ortega, A.M., Cubison, M.J., Froyd, K.D., Zhao, Y., Cliff, S.S., Hu, W.W., Toohey, D.W., Flynn, J.H., Lefer, B.L., Grossberg, N., Alvarez, S., Rappenglück, B., Taylor, J.W., Allan, J.D., Holloway, J.S., Gilman, J.B., Kuster, W.C., de Gouw, J.A., Massoli, P., Zhang, X., Liu, J., Weber, R.J., Corrigan, A.L., Russell, L.M., Isaacman, G., Worton, D.R., Kreisberg, N.M., Goldstein, A.H., Thalman, R., Waxman, E.M., Volkamer, R., Lin, Y.H., Surratt, J.D., Kleindienst, T.E., Offenberg, J. H., Dusanter, S., Griffith, S., Stevens, P.S., Brioude, J., Angevine, W.M., Jimenez, J. L., 2013. Organic aerosol composition and sources in Pasadena, California, during the 2010 CalNex campaign. J. Geophys. Res. Atmos. 118, 9233–9257. https://doi.org/10.1002/jgrd.50530.

He, Q., Bluvshtein, N., Segev, L., Meidan, D., Flores, J.M., Brown, S.S., Brune, W., Rudich, Y., 2018. Evolution of the complex refractive index of secondary organic aerosols during atmospheric aging. Environ. Sci. Technol. 52, 3456–3465. https:// doi.org/10.1021/acs.est.7b05742.

Heald, C.L., Kroll, J.H., Jimenez, J.L., Docherty, K.S., DeCarlo, P.F., Aiken, A.C., Chen, Q., Martin, S.T., Farmer, D.K., Artaxo, P., 2010. A simplified description of the evolution of organic aerosol composition in the atmosphere. Geophys. Res. Lett. 37. https://doi.org/10.1029/2010GL042737.

Hu, W., Day, D.A., Campuzano-Jost, P., Nault, B.A., Park, T., Lee, T., Croteau, P., Canagaratna, M.R., Jayne, J.T., Worsnop, D.R., Jimenez, J.L., 2018. Evaluation of the new capture vaporizer for Aerosol Mass Spectrometers (AMS): elemental composition and source apportionment of Organic Aerosols (OA). ACS Earth Space Chem. 2, 410–421. https://doi.org/10.1021/acsearthspacechem.8b00002.

Jensen, A.R., Koss, A.R., Hales, R.B., de Gouw, J.A., 2023. Measurements of volatile organic compounds in ambient air by gas-chromatography and real-time Vocus PTR-TOF-MS: calibrations, instrument background corrections, and introducing a PTR

- Data Toolkit. Atmos. Meas. Tech. 16, 5261–5285. https://doi.org/10.5194/amt-16-5261-2023
- Jimenez, J.L., Canagaratna, M.R., Donahue, N.M., Prevot, A.S.H., Zhang, Q., Kroll, J.H.,
 DeCarlo, P.F., Allan, J.D., Coe, H., Ng, N.L., Aiken, A.C., Docherty, K.S., Ulbrich, I.
 M., Grieshop, A.P., Robinson, A.L., Duplissy, J., Smith, J.D., Wilson, K.R., Lanz, V.A.,
 Hueglin, C., Sun, Y.L., Tian, J., Laaksonen, A., Raatikainen, T., Rautiainen, J.,
 Vaattovaara, P., Ehn, M., Kulmala, M., Tomlinson, J.M., Collins, D.R., Cubison, M.J.,
 E., Dunlea, J., Huffman, J.A., Onasch, T.B., Alfarra, M.R., Williams, P.I., Bower, K.,
 Kondo, Y., Schneider, J., Drewnick, F., Borrmann, S., Weimer, S., Demerjian, K.,
 Salcedo, D., Cottrell, L., Griffin, R., Takami, A., Miyoshi, T., Hatakeyama, S.,
 Shimono, A., Sun, J.Y., Zhang, Y.M., Dzepina, K., Kimmel, J.R., Sueper, D., Jayne, J.
 T., Herndon, S.C., Trimborn, A.M., Williams, L.R., Wood, E.C., Middlebrook, A.M.,
 Kolb, C.E., Baltensperger, U., Worsnop, D.R., 2009. Evolution of organic aerosols in
 the atmosphere. Science 326, 1525–1529. https://doi.org/10.1126/science.118035.
- Johnson, M.S., Strawbridge, K., Knowland, K.E., Keller, C., Travis, M., 2021. Long-range transport of Siberian biomass burning emissions to North America during FIREX-AQ. Atmos. Environ. 252, 118241. https://doi.org/10.1016/j.atmosenv.2021.118241.
- Jordan, A., Haidacher, S., Hanel, G., Hartungen, E., Märk, L., Seehauser, H., Schottkowsky, R., Sulzer, P., Märk, T.D., 2009. A high resolution and high sensitivity proton-transfer-reaction time-of-flight mass spectrometer (PTR-TOF-MS). Int. J. Mass Spectrom. 286, 122–128. https://doi.org/10.1016/j.ijms.2009.07.005.
- Kang, S., Hong, S., Lee, Y., Park, G., Park, T., Ban, J., Kim, K., Kim, Y., Choi, Y., Park, J., Ahn, J.-Y., Park, J., Yoo, M., Jeon, C.-S., Choi, J., Lee, T., 2025. Seasonal chemical characteristics and formation of potential secondary aerosols of a remote area in South Korea using an oxidation flow reactor. Atmos. Environ. 355, 121216. https://doi.org/10.1016/j.atmosenv.2025.121216.
- Laskin, A., Laskin, J., Nizkorodov, S.A., 2012. Mass spectrometric approaches for chemical characterisation of atmospheric aerosols: critical review of the most recent advances. Environ. Chem. 9, 163–189. https://doi.org/10.1071/EN12052.
- Li, F., Huang, D.D., Tian, L., Yuan, B., Tan, W., Zhu, L., Ye, P., Worsnop, D., Hoi, K.I., Mok, K.M., 2024. Response of protonated, adduct, and fragmented ions in Vocus proton-transfer-reaction time-of-flight mass spectrometer (PTR-ToF-MS). Atmos. Meas. Tech. 17, 2415–2427. https://doi.org/10.5194/amt-17-2415-2024.
- Li, M., Wang, T., Shu, L., Qu, Y., Xie, M., Liu, J., Wu, H., Kalsoom, U., 2021. Rising surface ozone in China from 2013 to 2017: a response to the recent atmospheric warming or pollutant controls? Atmos. Environ. 246, 118130. https://doi.org/ 10.1016/j.atmosenv.2020.118130.
- Li, R., Zhao, Y., Fu, H., Chen, J., Peng, M., Wang, C., 2021. Substantial changes in gaseous pollutants and chemical compositions in fine particles in the North China plain during the COVID-19 lockdown period: anthropogenic vs. meteorological influences. Atmos. Chem. Phys. 21, 8677–8692. https://doi.org/10.5194/acp-21-8677-2021.
- Li, S., Wang, S., Wu, Q., Zhang, Y., Ouyang, D., Zheng, H., Han, L., Qiu, X., Wen, Y., Liu, M., Jiang, Y., Yin, D., Liu, K., Zhao, B., Zhang, S., Wu, Y., Hao, J., 2023. Emission trends of air pollutants and CO2 in China from 2005 to 2021. Earth Syst. Sci. Data 15, 2279–2294. https://doi.org/10.5194/essd-15-2279-2023.
- Li, Y.J., Lee, B.P., Su, L., Fung, J.C.H., Chan, C.K., 2015. Seasonal characteristics of fine particulate matter (PM) based on high-resolution time-of-flight aerosol mass spectrometric (HR-ToF-AMS) measurements at the HKUST supersite in Hong Kong. Atmos. Chem. Phys. 15, 37–53. https://doi.org/10.5194/acp-15-37-2015.
- Liu, M., Huang, X., Song, Y., Xu, T., Wang, S., Wu, Z., Hu, M., Zhang, L., Zhang, Q., Pan, Y., Liu, X., Zhu, T., 2018. Rapid SO2 emission reductions significantly increase tropospheric ammonia concentrations over the north China plain. Atmos. Chem. Phys. 18, 17933–17943. https://doi.org/10.5194/acp-18-17933-2018.
- Lu, Z., Streets, D.G., Zhang, Q., Wang, S., Carmichael, G.R., Cheng, Y.F., Wei, C., Chin, M., Diehl, T., Tan, Q., 2010. Sulfur dioxide emissions in China and sulfur trends in east Asia since 2000. Atmos. Chem. Phys. 10, 6311–6331. https://doi.org/ 10.5194/acp-10-6311-2010.
- Mazzuca, G.M., Ren, X., Loughner, C.P., Estes, M., Crawford, J.H., Pickering, K.E., Weinheimer, A.J., Dickerson, R.R., 2016. Ozone production and its sensitivity to NOx and VOCs: results from the DISCOVER-AQ field experiment, Houston 2013. Atmos. Chem. Phys. 16, 14463–14474. https://doi.org/10.5194/acp-16-14463-2016.
- McMurry, P.H., 2000. A review of atmospheric aerosol measurements. Atmos. Environ. 34, 1959–1999. https://doi.org/10.1016/S1352-2310(99)00455-0.
- Nakaishi, T., 2021. Developing effective CO2 and SO2 mitigation strategy based on marginal abatement costs of coal-fired power plants in China. Appl. Energy 294, 116978. https://doi.org/10.1016/j.apenergy.2021.116978.
- Nault, B.A., Campuzano-Jost, P., Day, D.A., Schroder, J.C., Anderson, B., Beyersdorf, A. J., Blake, D.R., Brune, W.H., Choi, Y., Corr, C.A., de Gouw, J.A., Dibb, J., DiGangi, J. P., Diskin, G.S., Fried, A., Huey, L.G., Kim, M.J., Knote, C.J., Lamb, K.D., Lee, T., Park, T., Pusede, S.E., Scheuer, E., Thornhill, K.L., Woo, J.H., Jimenez, J.L., 2018. Secondary organic aerosol production from local emissions dominates the organic aerosol budget over Seoul, South Korea, during KORUS-AQ. Atmos. Chem. Phys. 18, 17769–17800. https://doi.org/10.5194/acp-18-17769-2018.
- Nault, B.A., Canagaratna, M., Croteau, P., Fortner, E., Lambe, A.T., Stark, H., Sueper, D., Werden, B.S., Williams, A., Williams, L.R., Worsnop, D., Jayne, J., DeCarlo, P.F., Cubison, M., Papadopoulos, G., Urs, R., 2025. Characterization of a new higher-resolution time-of-flight aerosol chemical speciation monitor: application for measurements of atmospheric aerosols. Aerosol. Sci. Technol. 59, 719–742. https://doi.org/10.1080/02786826.2025.2481221.
- Park, T., Choi, Y., Choi, J., Ahn, J., Park, J., Lee, Y., Ban, J., Park, G., Kang, S., Kim, K., Seo, B.-K., Kim, J., Park, S., Kim, H., Jeon, H., Lee, T., 2020. Aircraft measurements of physicochemical evolution of atmospheric aerosols in air pollution plumes over a megacity and suburban areas. Aerosol Air Qual. Res. 20, 2485–2494. https://doi.org/10.4209/aaqr.2019.12.0649.

- Piel, F., Müller, M., Mikoviny, T., Pusede, S.E., Wisthaler, A., 2019. Airborne measurements of particulate organic matter by proton-transfer-reaction mass spectrometry (PTR-MS): a pilot study. Atmos. Meas. Tech. 12, 5947–5958. https:// doi.org/10.5194/amt-12-5947-2019.
- Qi, L., Zheng, H., Ding, D., Wang, S., 2023. Responses of sulfate and nitrate to anthropogenic emission changes in eastern China - in perspective of long-term variations. Sci. Total Environ. 855, 158875. https://doi.org/10.1016/j. scitotenv.2022.158875.
- Raysoni, A.U., Pinakana, S.D., Luna, A., Mendez, E., Ibarra-Mejia, G., 2025. Characterization of BTEX species at Texas commission on environmental quality (TCEQ) continuous ambient monitoring station (CAMS) sites in Houston, Texas, USA during 2018. Sustain. Chem. Environ. 9, 100227. https://doi.org/10.1016/j. sceny.2025.100227
- Sahu, L.K., Yadav, R., Tripathi, N., 2020. Aromatic compounds in a semi-urban site of Western India: seasonal variability and emission ratios. Atmos. Res. 246, 105114. https://doi.org/10.1016/j.atmosres.2020.105114.
- Schroder, J.C., Campuzano-Jost, P., Day, D.A., Shah, V., Larson, K., Sommers, J.M., Sullivan, A.P., Campos, T., Reeves, J.M., Hills, A., Hornbrook, R.S., Blake, N.J., Scheuer, E., Guo, H., Fibiger, D.L., McDuffie, E.E., Hayes, P.L., Weber, R.J., Dibb, J. E., Apel, E.C., Jaeglé, L., Brown, S.S., Thornton, J.A., Jimenez, J.L., 2018. Sources and secondary production of organic aerosols in the northeastern United States during WINTER. J. Geophys. Res. Atmos. 123, 7771–7796. https://doi.org/10.1029/2018.JD028475.
- Silva, R.A., West, J.J., Zhang, Y., Anenberg, S.C., Lamarque, J.-F., Shindell, D.T., Collins, W.J., Dalsoren, S., Faluvegi, G., Folberth, G., Horowitz, L.W., Nagashima, T., Naik, V., Rumbold, S., Skeie, R., Sudo, K., Takemura, T., Bergmann, D., Cameron-Smith, P., Cionni, I., Doherty, R.M., Eyring, V., Josse, B., MacKenzie, I.A., Plummer, D., Righi, M., Stevenson, D.S., Strode, S., Szopa, S., Zeng, G., 2013. Global premature mortality due to anthropogenic outdoor air pollution and the contribution of past climate change. Environ. Res. Lett. 8, 034005. https://doi.org/10.1088/1748-9326/8/3/034005.
- Song, M., He, S., Li, X., Liu, Y., Lou, S., Lu, S., Zeng, L., Zhang, Y., 2024. Optimizing the iodide-adduct chemical ionization mass spectrometry (CIMS) quantitative method for toluene oxidation intermediates: experimental insights into functional-group differences. Atmos. Meas. Tech. 17, 5113–5127. https://doi.org/10.5194/amt-17-5113-2024
- Song, S., Gao, M., Xu, W., Sun, Y., Worsnop, D.R., Jayne, J.T., Zhang, Y., Zhu, L., Li, M., Zhou, Z., Cheng, C., Lv, Y., Wang, Y., Peng, W., Xu, X., Lin, N., Wang, Y., Wang, S., Munger, J.W., Jacob, D.J., McElroy, M.B., 2019. Possible heterogeneous chemistry of hydroxymethanesulfonate (HMS) in northern China winter haze. Atmos. Chem. Phys. 19, 1357–1371. https://doi.org/10.5194/acp-19-1357-2019.
- Sullivan, A.P., Guo, H., Schroder, J.C., Campuzano-Jost, P., Jimenez, J.L., Campos, T., Shah, V., Jaeglé, L., Lee, B.H., Lopez-Hilfiker, F.D., Thornton, J.A., Brown, S.S., Weber, R.J., 2019. Biomass burning markers and residential burning in the WINTER aircraft campaign. J. Geophys. Res. Atmos. 124, 1846–1861. https://doi.org/10.1029/2017JD028153.
- Sun, Y.L., Wang, Z.F., Du, W., Zhang, Q., Wang, Q.Q., Fu, P.Q., Pan, X.L., Li, J., Jayne, J., Worsnop, D.R., 2015. Long-term real-time measurements of aerosol particle composition in beijing, China: seasonal variations, meteorological effects, and source analysis. Atmos. Chem. Phys. 15, 10149–10165. https://doi.org/10.5194/acp-15-10149-2015.
- Thapa, P., Xu, J., Neupane, B., Rupakheti, D., 2020. Chemical composition of inorganic and organic species in snow/ice in the glaciers of Western China. Sci. Total Environ. 706, 135351. https://doi.org/10.1016/j.scitotenv.2019.135351.
 Wang, L., Liu, Z., Sun, Y., Ji, D., Wang, Y., 2015. Long-range transport and regional
- Wang, L., Liu, Z., Sun, Y., Ji, D., Wang, Y., 2015. Long-range transport and regional sources of PM2.5 in beijing based on long-term observations from 2005 to 2010. Atmos. Res. 157, 37–48. https://doi.org/10.1016/j.atmosres.2014.12.003.
- Wang, S., Gallimore, P.J., Liu-Kang, C., Yeung, K., Campbell, S.J., Utinger, B., Liu, T., Peng, H., Kalberer, M., Chan, A.W.H., Abbatt, J.P.D., 2023. Dynamic wood smoke aerosol toxicity during oxidative atmospheric aging. Environ. Sci. Technol. 57, 1246–1256. https://doi.org/10.1021/acs.est.2c05929.
- Wang, Y., Eriksson, T., Luo, N., 2023. The health impacts of two policies regulating SO2 air pollution: evidence from China. China Econ. Rev. 78, 101937. https://doi.org/ 10.1016/j.chieco.2023.101937.
- Warneke, C., Schwarz, J.P., Dibb, J., Kalashnikova, O., Frost, G., Al-Saad, J., Brown, S.S., Brewer, W.A., Soja, A., Seidel, F.C., Washenfelder, R.A., Wiggins, E.B., Moore, R.H., Anderson, B.E., Jordan, C., Yacovitch, T.I., Herndon, S.C., Liu, S., Kuwayama, T., Jaffe, D., Johnston, N., Selimovic, V., Yokelson, R., Giles, D.M., Holben, B.N., Goloub, P., Popovici, I., Trainer, M., Kumar, A., Pierce, R.B., Fahey, D., Roberts, J., Gargulinski, E.M., Peterson, D.A., Ye, X., Thapa, L.H., Saide, P.E., Fite, C.H., Holmes, C.D., Wang, S., Coggon, M.M., Decker, Z.C.J., Stockwell, C.E., Xu, L., Gkatzelis, G., Aikin, K., Lefer, B., Kaspari, J., Griffin, D., Zeng, L., Weber, R., Hastings, M., Chai, J., Wolfe, G.M., Hanisco, T.F., Liao, J., Campuzano Jost, P., Guo, H., Jimenez, J.L., Crawford, J., Team, T.F.-A.S., 2023. Fire influence on regional to global environments and air quality (FIREX-AQ). J. Geophys. Res. Atmos. 128, e2022JD037758. https://doi.org/10.1029/2022JD037758.
- Wen, L., Xue, L., Dong, C., Wang, X., Chen, T., Jiang, Y., Gu, R., Zheng, P., Li, H., Shan, Y., Zhu, Y., Zhao, Y., Yin, X., Liu, H., Gao, J., Wu, Z., Wang, T., Herrmann, H., Wang, W., 2023. Reduced atmospheric sulfate enhances fine particulate nitrate formation in eastern China. Sci. Total Environ. 898, 165303. https://doi.org/ 10.1016/j.scitotenv.2023.165303.
- Winijkul, E., Bond, T.C., 2016. Emissions from residential combustion considering enduses and spatial constraints: part II, emission reduction scenarios. Atmos. Environ. 124, 1–11. https://doi.org/10.1016/j.atmosenv.2015.10.011.

- Wu, L., Wang, Y., Li, L., Zhang, G., 2020. Acidity and inorganic ion formation in PM2.5 based on continuous online observations in a south China megacity. Atmos. Pollut. Res. 11, 1339–1350. https://doi.org/10.1016/j.apr.2020.05.003.
- You, H., Li, N., Gao, C.-k., Liu, C., Chen, Z.-j., Bai, L., Li, Y., 2025. Village-level emission inventory of residential coal combustion and reduction analysis: a case study of Liaoning Province, China. Renew. Sustain. Energy Rev. 208, 115046. https://doi. org/10.1016/j.rser.2024.115046.
- Zawadowicz, M.A., Suski, K., Liu, J., Pekour, M., Fast, J., Mei, F., Sedlacek, A.J., Springston, S., Wang, Y., Zaveri, R.A., Wood, R., Wang, J., Shilling, J.E., 2021. Aircraft measurements of aerosol and trace gas chemistry in the eastern north Atlantic. Atmos. Chem. Phys. 21, 7983–8002. https://doi.org/10.5194/acp-21-7983-2021
- Zhang, W., Xu, L., Zhang, H., 2024. Recent advances in mass spectrometry techniques for atmospheric chemistry research on molecular-level. Mass Spectrom. Rev. 43, 1091–1134. https://doi.org/10.1002/mas.21857.
- Zheng, B., Tong, D., Li, M., Liu, F., Hong, C., Geng, G., Li, H., Li, X., Peng, L., Qi, J., Yan, L., Zhang, Y., Zhao, H., Zheng, Y., He, K., Zhang, Q., 2018. Trends in China's

- anthropogenic emissions since 2010 as the consequence of clean air actions. Atmos. Chem. Phys. 18, 14095–14111. https://doi.org/10.5194/acp-18-14095-2018.
- Zhong, H., Huang, R.J., Lin, C., Xu, W., Duan, J., Gu, Y., Huang, W., Ni, H., Zhu, C., You, Y., Wu, Y., Zhang, R., Ovadnevaite, J., Ceburnis, D., O'Dowd, C.D., 2022. Measurement report: on the contribution of long-distance transport to the secondary aerosol formation and aging. Atmos. Chem. Phys. 22, 9513–9524. https://doi.org/10.5194/acn-22-9513-2022
- Zhou, M., Zheng, G., Wang, H., Qiao, L., Zhu, S., Huang, D., An, J., Lou, S., Tao, S., Wang, Q., Yan, R., Ma, Y., Chen, C., Cheng, Y., Su, H., Huang, C., 2022. Long-term trends and drivers of aerosol pH in eastern China. Atmos. Chem. Phys. 22, 13833–13844. https://doi.org/10.5194/acp-22-13833-2022.
- Zografou, O., Gini, M., Fetfatzis, P., Granakis, K., Foskinis, R., Manousakas, M.I., Tsopelas, F., Diapouli, E., Dovrou, E., Vasilakopoulou, C.N., Papayannis, A., Pandis, S.N., Nenes, A., Eleftheriadis, K., 2024. High-altitude aerosol chemical characterization and source identification: insights from the CALISHTO campaign. Atmos. Chem. Phys. 24, 8911–8926. https://doi.org/10.5194/acp-24-8911-2024.